Talanta 186 (2018) 238–247

Contents lists available at ScienceDirect

Talanta

journal homepage: www.elsevier.com/locate/talanta

Highly selective and sensitive chemiluminescence biosensor for adenosine detection based on carbon quantum dots catalyzing luminescence released from aptamers functionalized graphene@magnetic β-cyclodextrin polymers

Yuanling Sun, Chaofan Ding, Yanna Lin, Weiyan Sun, Hao Liu, Xiaodong Zhu, Yuxue Dai, Chuannan Luo*

Key Laboratory of Interfacial Reaction & Sensing Analysis in Universities of Shandong, School of Chemistry and Chemical Engineering, University of Jinan, Jinan 250022, PR China

ARTICLE INFO

Keywords:
Chemiluminescence
β-cyclodextrin
Graphene
Adenosine
CQDs

ABSTRACT

In this work, a highly selective and sensitive chemiluminescence (CL) biosensor was prepared for adenosine (AD) detection based on carbon quantum dots (CQDs) catalyzing the CL system of luminol-H_2O_2 under alkaline environment and CQDs was released from the surface of AD aptamers functionalized graphene @ magnetic β-cyclodextrin polymers (GO@Fe_3O_4@β-CD@A-Apt). Firstly, GO@Fe_3O_4@β-CD and CQDs were prepared and characterized by transmission electron microscopy (TEM), scanning electron microscope (SEM), UV–Vis absorption spectra (UV), fluorescence spectra (FL), fourier transform infrared (FTIR) and X-ray powder diffraction (XRD). For GO@Fe_3O_4@β-CD, Fe_3O_4 was easy to separate, GO had good biocompatibility and large specific surface area, and β-CD further increased the specific surface area of the adenosine polymers (A-Apt) to provided larger binding sites to A-Apt. Then, A-Apt was modified on the surface of GO@Fe_3O_4@β-CD while CQDs was modified by ssDNA (a single stranded DNA partially complementary to A-Apt). The immobilization property (GO@Fe_3O_4@β-CD to A-Apt) and the adsorption property (GO@Fe_3O_4@β-CD@A-Apt to CQDs-ssDNA) were sequentially researched. The base-supported chain-like polymers – GO@Fe_3O_4@β-CD@A-Apt/CQDs-ssDNA was successfully obtained. When AD existed, CQDs-ssDNA was released from the surface of GO@Fe_3O_4@β-CD@A-Apt and catalyzed CL. After that, under optimized CL conditions, AD could be measured with the linear concentration range of 5.0×10^{-13}–5.0×10^{-9} mol/L and the detection limit of 2.1×10^{-13} mol/L (3δ) while the relative standard deviation (RSD) was 1.4%. Finally, the GO@Fe_3O_4@β-CD@A-Apt/CQDs-ssDNA-CL biosensor was used for the determination of AD in urine samples and recoveries ranged from 98.6% to 101.0%. Those satisfactory results illustrated the proposed CL biosensor could achieve highly selective, sensitive and reliable detection of AD and revealed potential application for AD detection in monitoring and diagnosis of human cancers.

1. Introduction

Adenosine (AD) is an endogenous nucleoside throughout of human cells and has aroused medical researchers' interest since it was discovered. AD is not only an important intermediate for the synthesis of adenosine triphosphate (ATP), adenine, adenylate and adenosine, but also can produce adenylate, participate in myocardial energy metabolism and expand the coronary blood vessels [1,2]. In addition, many studies have shown that AD can be used as a potential biomarker of cancers or tumors, which shows a good clinical practice value in broad-spectrum cancer diagnosis and surgical efficacy evaluation [3,4]. Therefore, the detection of AD is of great significance. At present, common methods for detection of AD have colorimetric [5], surface enhanced raman scattering (SERS) [6], electrochemical [7], fluorescence [8], fluorescence resonance energy transfer (FRET) [9], reversed-phase high-performance liquid chromatography (RP-HPLC) [10], resonance light scattering (RLS) [11], chemiluminescence (CL) [12,13]. But some of the above-mentioned methods also have some drawbacks, such as expensive instruments, complex operation, limited detection range and weak anti-interference ability. So, finding a more simple, cost-effective, sensitive and selective method to detect AD is significant important.

CL is defined as a kind of emissive light through chemical reactions [14]. Compared with other analytical methods, CL has many significant

* Corresponding author.
E-mail address: chm_yfl518@163.com (C. Luo).

https://doi.org/10.1016/j.talanta.2018.04.068
Received 17 January 2018; Received in revised form 14 April 2018; Accepted 20 April 2018
Available online 23 April 2018
0039-9140/

advantages, such as no need external light source, simple instrument, high sensitivity, wide detection range and easy to achieve automation [15]. Based on these advantages, CL has been used in biomedical [16], environmental monitoring [17] quality assessment [18], sensing analysis [19] and other fields. However, because the substances present in samples can easily affect the CL intensity, the application of CL technology is restricted by its low selectivity which could be improved by bringing some specific recognizable materials into the system, such as molecularly imprinted polymers [20], special frame materials [21], specific biomaterials [22].

The CL intensity (I) of the pure chemical reaction is quite weak, so catalysts are usually used in CL technology. Common catalysts used in CL are a variety of metal ions and enzymes (including some simulated enzymes) [23]. Among these catalysts, semiconductor nano-materials, also known as quantum dots (QDs), have attracted researchers' wide attention due to their unique optical properties [24]. Among these QDs, carbon quantum dots (CQDs) can be used as photoelectron transfer to the electron donor or receptor owing to its strong light energy conversion, so CQDs has been widely used in the field of photocatalysis [25]. CQDs with highly photoluminescent were successfully prepared and were applied to the construction of accurate ratiometric sensor for detection of Hg^{2+} and biological thiols by You et al. [26]. CQDs were used to the determination of cytochrome and displayed strong cathodic electrogenerated chemiluminescence (ECL) in neutral aqueous solution in the presence of potassium persulfate by Dong et al. [27].

Aptamers (Apt) are a kind of synthetic single-stranded oligonucleotides screened by SELEX technology [28]. Apt can efficiently and specifically bind to target molecules and its appearances provide an efficient and rapid identification of the research platform in the field of biology and biomedical sciences [29,30]. At present, biomolecule detection is usually based on the mode of antigen-specific antibody recognition, but the applications of antibodies are usually limited due to its easy inactivation and long preparation time. In contrast, Apt has its own advantages of good stability, easy to obtain, relatively simple and fast preparation synthesis, easy to functional modification and labeling. Therefore, Apt has been widely used in the construction of biosensors. Li et al. [31] proposed a novel ultrasensitive one-compartment enzyme biofuel cells (EBFCs)-based self-powered aptasensing platform for antibiotic residue detection. A reusable aptasensor of human thrombin was constructed based on an extension-contraction movement of DNA interconversion based on resonance light scattering technique using magnetic nanoparticles as the probe by Yue et al. [32].

Graphene (GR) is a two-dimensional carbon nanomaterial and its thickness is only 0.335 nm, known as the thinnest material in the world [33]. GR has a complete and stable six-membered ring structure to make it chemically inert and hydrophobic, so it difficult to disperse in a polar solvent or aqueous solution, which limits the application of GR. It is necessary to make modification to broaden its scope of application. Graphene oxide (GO) is an important derivative of GR, which has the basically similar structure to GR, and GO contains abundant carboxylic acid, epoxy group and hydroxyl group [34]. As an amphiphilic lamellar molecule, GO shows excellent biocompatibility that make it and its derivatives could be used in analytical detection [35], polymer materials synthesis [36], biomedicine [37], photoelectric applications [38] and other fields. Especially, GO and its composites have been widely used in the preparation of sensors [39]. For examples, Ling et al. [40] developed a simple, sensitive, selective turn-on fluorescent aptasensor for theophylline detection in serum by utilizing ligand-induced self-assembling RNA aptamers and two different interaction stages of the aptamers fragments with GO. GO was modified on the surface of glassy carbon electrode (GCE) and it was successfully used to construction of the new electrochemical sensor for acetaminophen detection by Song et al. [41].

Cyclodextrin (CD) is a cyclic oligosaccharide compound that formed by a number of D-glucopyranose units. The whole molecule of CD exhibits a narrow half-tapered cavity structure owing to the glucose units of CD with non-twisted chair conformations [42,43]. There are three kinds common CDs – α-CD, β-CD, γ-CD, of which β-CD is the most widely used because of its caliber moderate size, low production costs, raw material easy to get and product [44]. However, the unmodified β-CD still has some disadvantages, such as limited bonding ability, poor solubility in organic solvents and low catalytic activity, which limits its widely use. In order to change this situation, its derivatives or complex are composited [45] and has been widely used in environmental treatment [46], drug delivery [47], biosensing analysis [48] and other fields.

In this study, GO@Fe_3O_4@β-CD and CQDs were synthesized and characterized. A-Apt and CQDs-ssDNA were consecutively modified to the surface of GO@Fe_3O_4@β-CD to synthesize the final base-supported chain-like polymers – GO@Fe_3O_4@β-CD@A-Apt/CQDs-ssDNA and the polymers were applied to detect AD by CL method. When AD existed in solutions, CQDs-ssDNA was released from the surface of GO@Fe_3O_4@β-CD@A-Apt owing to the specific recognition ability between AD and A-Apt and the released CQDs-ssDNA catalyzed CL. Ultimately, a highly selective, sensitive and simple GO@Fe_3O_4@β-CD@A-Apt/CQDs-ssDNA - CL biosensor was successful constructed and realized the detection of AD.

2. Experimental

2.1. Materials

AD aptamers: 5′-GTCTCTGTGTGCGCCAGAGAACACTGGGGCAGATATG GGCCAGCACAGAATGAGGCCC-3′ (10 OD) and ssDNA : 5′-CTCC GGGCGGA GGAAGGTGTCACA-3′ (5 OD) were purchased from Sangon Biotech Company (Shanghai, China). Graphite powder was supplied by Hongyan Chemical Reagent Factory (Tianjin, China). β-CD was supplied by Kermel Chemical Reagent Co., Ltd. (Tianjin, China). Ferrous chloride and ferric chloride were purchased from Sinopharm Chemical Reagent Co., Ltd. (Beijing, China). Epichlorohydrin (ECH), Aminopropyltriethoxysilane (APTS) and chitosan (CS) were provided by Shanghai Macklin Biochemicals Co., Ltd. (Shanghai, China). 1-(3-dimethylaminopropyl)-3-ethylcarbodiimide Luminol (EDC) and N-hydroxysuccinimide (NHS) were purchased from Sass chemical technology Co., Ltd (Shanghai, China). Adenosine was supplied by Mengyi beauty Biotechnology Co. Ltd. (Beijing, China). Bovine serum albumin (BSA), creatinine (Cr), glycine (Gly) and other biological interferences were purchased from Solebo Biological Technology Co. Ltd. (Beijing, China). Anhydrous toluene purchased from Tianjin Fuyu Fine Chemical Co., Ltd. (Tianjin, China). Acetic acid, Sodium hydroxide, Potassium permanganate, ethanol and all other chemicals unless specified were analytical reagent grade and used without further purification. Redistilled water was used throughout the work. Phosphate buffer (PBS, pH = 7.4, 0.01 mol/L) solution was used to prepare all AD solutions in all the experiment.

2.2. Apparatus

The IFFM-E flow injection CL analyzer (Xi'an Remex Electronic instrument High-Tech Ltd, China) was equipped with an automatic injection system and a detection system. As shown in Fig. 1, in the flow injection system, luminol and NaOH flowed into the mixing reaction system through the two channels of main pump with the flow rate of 1.69 mL/min, respectively. Meanwhile, H_2O_2 and samples (or PBS) flowed through two channels of the vice pump with the flow rate of 1.45 mL/min, respectively. When AD samples were detected, a certain amount of GO@Fe_3O_4@β-CD@A-Apt/ CQDs-ssDNA dispersion was placed in AD sample and a magnet was placed in the bottom of sample tube to achieve magnetic separation. The supernatant after magnetic separation flowed into the IFFM-E flow injection CL analyzer system. It took only 311 s to complete a test and can yield five parallel data peaks simultaneously. All samples tests were carried out the optimized

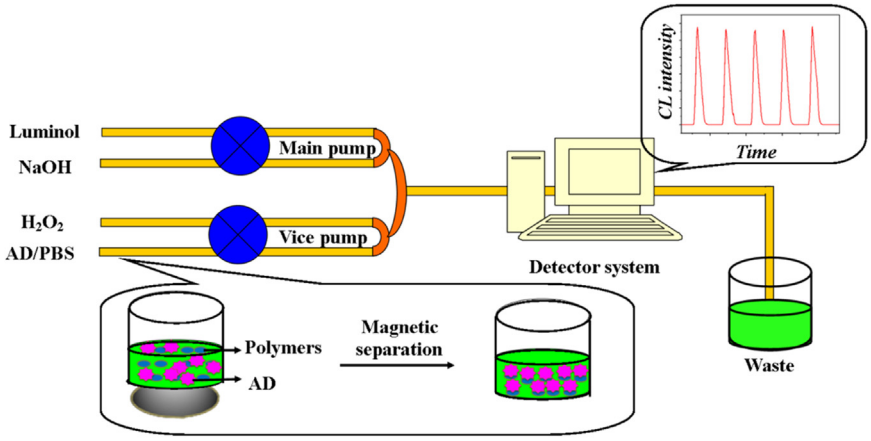

Fig. 1. The schematic of IFFM-E flow injection chemiluminescence analyzer.

conditions: the solution flow rate in the main pump of 1.69 mL/min, the solution flow rate in the vice pump of 1.45 mL/min, 5.0×10^{-4} mol/L of luminol, 0.1 mol/L of H_2O_2 and 0.02 mol/L of NaOH, simultaneously. The schematic of IFFM-E flow injection chemiluminescence analyzer was shown in Fig. 1.

2.3. Preparation of GO

GO was prepared by a modified Hummers procedure described in previous literatures from other researchers [49] and our group [50], respectively. Firstly, 1.0 g of graphite powder was added into a 500 mL of three mouth flask, in which 200 mL of mixed acid (V_{H2SO4}:V_{HNO3} = 8:1) was put in advance. Then 6.0 g of potassium permanganate was added and the diluted suspension was stirred for 12 h at 90 °C. Subsequently, 30% of H_2O_2 was dropped till no bubbles were produced (no reaction). Finally, the mixture was centrifuged and washed by 0.2 mol/L HCl and water, respectively. After vacuum dried at 60 °C, the product was obtained.

2.4. Preparation of Fe_3O_4@β-CD

2.4.1. Preparation of Fe_3O_4

0.01 mol of $FeCl_2$ and 0.02 mol of $FeCl_3$ were mixed and dissolved in 100 mL of water. Then 10 mL of ammonia was added and the mixture was stirred for 60 min under the atmosphere of N_2 at 90 °C. Lastly, the product was separated by the external magnetic field and washed by water.

2.4.2. Preparation of Fe3O4@β-CD

The above synthetic magnetic particles were added to 50 mL 0.08 g/mL of β-CD that was dissolved by 0.05 mol/L of sodium hydroxide solution. After ultrasonic dispersion for 20 min, 10 mL of ECH was slowly added and mechanically stirred for 1 h at 65 °C. Then the mixture was separated by the external magnetic field and washed by water. The final product was dried at 60 °C.

2.5. Preparation of GO@Fe_3O_4@β-CD

2.5.1. Amination of Fe_3O_4@β-CD

0.5 g of Fe_3O_4@β-CD was added to a mixture of 5 mL of APTS and 20 mL of anhydrous toluene and heated for 12 h under the atmosphere of N_2. The product was collected with an external magnetic field and washed by water. After vacuum dried at 60 °C, the silanized product was obtained.

2.5.2. Preparation of GO@Fe_3O_4@β-CD

0.2 g of GO was dissolved to 100 mL of water in a 500 mL of three mouth flask. Subsequently, 3 mg of EDC and 28 mg of NHS were added to the dispersion. After magnetic stirring and ultrasonic to form a uniform dispersion, 200 mg of aminated Fe_3O_4@β-CD was added and ultrasound dispersion for 30 min. Then the mixture was stirred for 2 h at 80 °C. After magnetic separation, washed by water and dried. The final product – GO@Fe_3O_4@β-CD was successful prepared.

2.6. Preparation of CQDs-ssDNA

2.6.1. Preparation of CQDs

CQDs are prepared by solvent thermal reaction. 2.5 g of chitosan was dissolved into the mixed solution of 22 mL 36% of acetic acid and 13 mL of water. The solution was transferred to a 50 mL of autoclave and reacted for 12 h at 180 °C. Finally, after centrifugal separation, washed by water and dried, CQDs was obtained.

2.6.2. Preparation of CQDs-ssDNA

0.5 mL of 1.5×10^{-5} mol/L of the above-prepared CQDs and a certain amount of ssDNA were added to a 50 mL of beaker. Then the mixture was shaken to make it fully mixed and placed in the dark for 1 h. Finally, 0.1% BSA was added and placed for 1 h in order to prevent nonspecific adsorption in subsequent experiments and the solution was dissolved with PBS buffer in a 500 mL of volumetric flask. So 1.5×10^{-8} mol/L CQDs-ssDNA was prepared and stored at 4 °C in a refrigerator. The preparation process of the polymers was shown in Fig. 2.

2.7. Immobilization/adsorption experiment of polymers

The static method of investigating immobilization performance of GO@Fe_3O_4@β-CD to A-Apt (adsorption performance of GO@Fe_3O_4@β-CD@A-Apt to CQDs-ssDNA) involved the determination of various concentrations of A-Apt (CQDs-ssDNA) for defined incubation periods and the determination of A-Apt (CQDs-ssDNA) concentration in different incubation periods.

2.7.1. Immobilization isotherm

Many parallel 5.0 mL of 0.1 g/L GO@Fe_3O_4@β-CD dispersions were placed into 50 mL colorimetric tubes, respectively. Then, different volume doses of 4.0×10^{-9} mol/L of A-Apt solutions were added to the tubes, respectively. Then these tubes were shaken at 25 °C for 1 h. After magnetic separation, the concentrations of the supernatant in tubes were determined by a CL instrument and the immobilization capacities were calculated.

2.7.2. Immobilization dynamics

Many parallel 5.0 mL of 0.1 g/L GO@Fe_3O_4@β-CD dispersions were

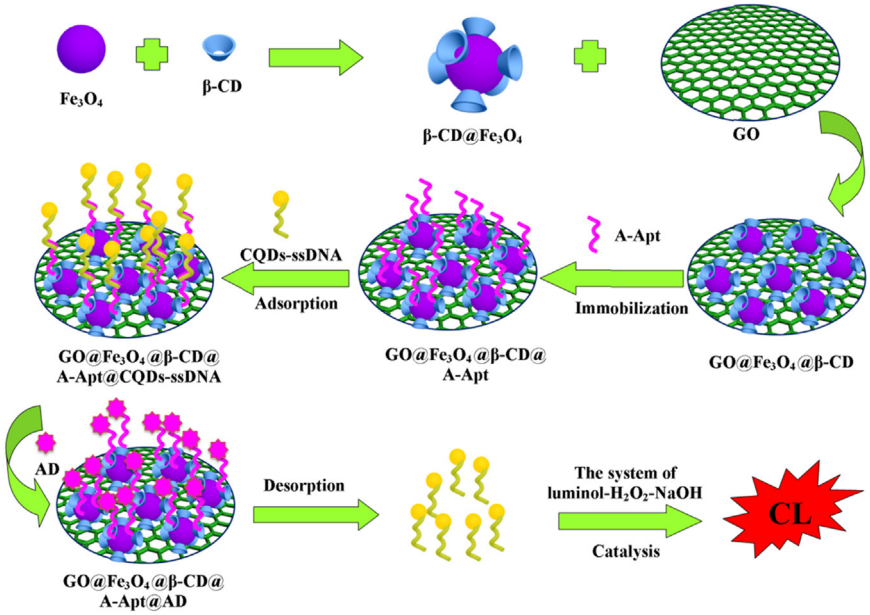

Fig. 2. The preparing process of GO@Fe_3O_4@β-CD@A-Apt and the schematic diagram construction of GO@Fe_3O_4@β-CD@A-Apt/CQDs-ssDNA-CL biosensor.

dispersed in 25.0 mL 4.0 × 10^{-9} mol/L of A-Apt solution, which then were shaken for 0.5 min, 1 min, 3 min, 5 min, 8 min, 10 min, 15 min, 20 min, 25 min and 30 min, respectively. After magnetic separation, the concentrations of the supernatant in tubes were determined by a CL instrument and the immobilization capacities were calculated.

2.7.3. Calculation formula of immobilization capacity

The immobilization capacity was calculated from the following formula:

$$Q_e = (c_0 - c_e)V/m$$

where Q_e (mol/mg) was the mass of A-Apt immobilized per unit mass of GO@Fe_3O_4@β-CD; c_0 (mol/L) and c_e (mol/L) were the A-Apt concentrations of the initial and balance solution, respectively; V (L) was the total volume of the immobilization mixture and m (mg) was the addition of GO@Fe_3O_4@β-CD.

2.7.4. Adsorption isotherm

Many parallel 5.0 mL of 0.1 g/L GO@Fe_3O_4@β-CD @A-Apt dispersions were placed into 50 mL colorimetric tubes, respectively. Then, different volume doses of 1.5 × 10^{-8} mol/L of CQDs-ssDNA solution were added to the tubes, respectively, and the tubes were shaken at 25 °C for 1 h. After magnetic separation, the concentration of the supernatant in the tubes was determined by a CL instrument and the adsorption capacities were calculated.

2.7.5. Rebinding dynamics

Many parallel 5.0 mL of 0.1 g/L GO@Fe_3O_4@β-CD @A-Apt dispersions was dispersed in 6.0 mL of 1.5 × 10^{-8} mol/L of CQDs-ssDNA solution, which then were shaken for 0.5 min, 1 min, 3 min, 5 min, 8 min, 10 min, 15 min, 20 min, 25 min and 30 min, respectively. After magnetic separation, the concentration of the supernatant in the tube was determined by a CL instrument and the adsorption capacities were calculated.

2.7.6. Calculation formula of adsorption capacity

The adsorption capacity was calculated from the following formula:

$$Q'_e = (c'_0 - c'_e)V'/m'$$

where Q'_e (mol/mg) was the mass of CQDs-ssDNA adsorbed per unit mass of GO@Fe_3O_4@β-CD@A-Apt; c'_0 (mol/L) and c'_e (mol/L) were the concentrations of the initial and balance solution, respectively; V' (L) was the total volume of the adsorption mixture and m' (mg) was the addition of GO@Fe_3O_4@β-CD@A-Apt.

2.8. Selectivity experiment of the CL biosensor

To study selectivity of the GO@Fe_3O_4@β-CD@A-Apt/CQDs-ssDNA-CL biosensor, the selectivity experiment was carried out. In the experiment, different amounts of interference substances were added into AD standard solution (c_{AD}: 5.0 × 10^{-13} mol/L) to research its effects on the CL intensity. These effects were reflected by the interference multiples, which was a multiples value of the concentration of interferences relative to the concentration of AD. Interference substances in the experiment were simulate urine components, such as uric acid (UA), creatinine (Cr), glycine (Gly), L-cysteine (L-Cys), ammonium carbonate (AC), Lactic acid (LA), potassium ion (K^+) and chloride ion (Cl^-).

2.9. Recyclability experiment of the CL biosensor

In order to investigate the practicality of the GO@Fe_3O_4@β-CD@A-Apt/CQDs-ssDNA-CL biosensor, the recyclability of GO@Fe_3O_4@β-CD, as an important parameter of the biosensor, was researched by comparing the immobilization capacities of the GO@Fe_3O_4@β-CD that were used different times to A-Apt. In the experiment, A-Apt was immobilized on the surface of GO@Fe_3O_4@β-CD by the π-π stacking effect between CS@Fe_3O_4@GO and A-Apt. Different immobilization capacities of A-Apt caused the different changes of CL intensity.

2.10. Detection process of samples

AD samples were detected by the following procedure.

First of all, only PBS solution was filled in the sample tube and the blank CL intensity of I_0 was measured.

Then, AD sample existed in the sample tube. The CL signal I_1 was obtained and $\Delta I_1 = I_1 - I_0$ was the CL intensity produced by the whole AD samples (interferences inside).

Lastly, GO@Fe_3O_4@β-CD@A-Apt/CQDs-ssDNA was added to AD sample in sample tube. AD could be specific absorbed by the polymers via the strong specificity effect between A-Apt and AD. CQDs-ssDNA was desorbed from the surface of GO@Fe_3O_4@β-CD@A-Apt and catalyzed CL. So another CL signal I_2 could be obtained and $\Delta I_2 = I_2 - I_0$

was proportional to AD concentration.

The final $\Delta I = \Delta I_2 - \Delta I_1$ was the actual CL signal of the target analyte – AD. So the specific recognition and measurement system of AD detection was constituted.

3. Results and discussion

3.1. Characterization of synthetic materials

As shown in Fig. 3, the surface morphology of the CQDs, Fe_3O_4, Fe_3O_4@β-CD, GO and GO@Fe_3O_4@β-CD were characterized. As shown in Fig. 3(A), CQDs presented small black spots with relatively uniform size and the diameter of around 5 nm. In Fig. 3(B), the prepared Fe_3O_4 showed relatively regular spherical and had good dispersion. From the TEM/SEM image of Fe_3O_4@β-CD in Fig. 3(C, D), it showed that the surface of Fe_3O_4 had a relatively clear coating layer of β-CD. In Fig. 3(E), a wrinkled and thin film was observed in the image of GO, which demonstrated the large specific surface area of GO. Fig. 3(F) clearly reveals that the surface of GO successfully modified on the spherical structure which contributed to Fe_3O_4@β-CD and indicated the successfully synthesis of GO@Fe_3O_4@β-CD.

Subsequently, the FL and UV characterizations of CQDs were shown in Fig. 4(A). The FL characteristic absorption peak of CQDs appeared at 435 nm under the excitation wavelength of 360 nm while the UV spectra showed a characteristic absorption peak at 265 nm, which was the characteristic UV absorption peak of CQDs [51]. Thus, CQDs were successfully synthesized.

Then, Fig. 4(B) showed the FTIR of GO, Fe_3O_4, Fe_3O_4@β-CD and GO@Fe_3O_4@β-CD under the wavenumber range of 400–4000 cm^{-1}. In these spectrums, a broad and strong absorption peak appeared at 3445 cm^{-1}, which belongs to the stretching vibration peak of –OH. In the spectrums of GO, the absorption peaks at 1703 cm^{-1}, 1380 cm^{-1} and 1055 cm^{-1} belong to the stretching vibration peak of C=O, the deformation vibration peak O-H and the stretching vibration peak of C-O, respectively. These results showed that different kinds of oxygen-containing functional groups existed in the surface of the composite and GO was successfully synthesized. In the spectrum of Fe_3O_4, a strong absorption peak appeared around 600 cm^{-1}, which is the characteristic absorption peak of Fe_3O_4. In the characterization curve of Fe_3O_4@β-CD, 600 cm^{-1} was the characteristic absorption peak of Fe_3O_4, 1049 cm^{-1}

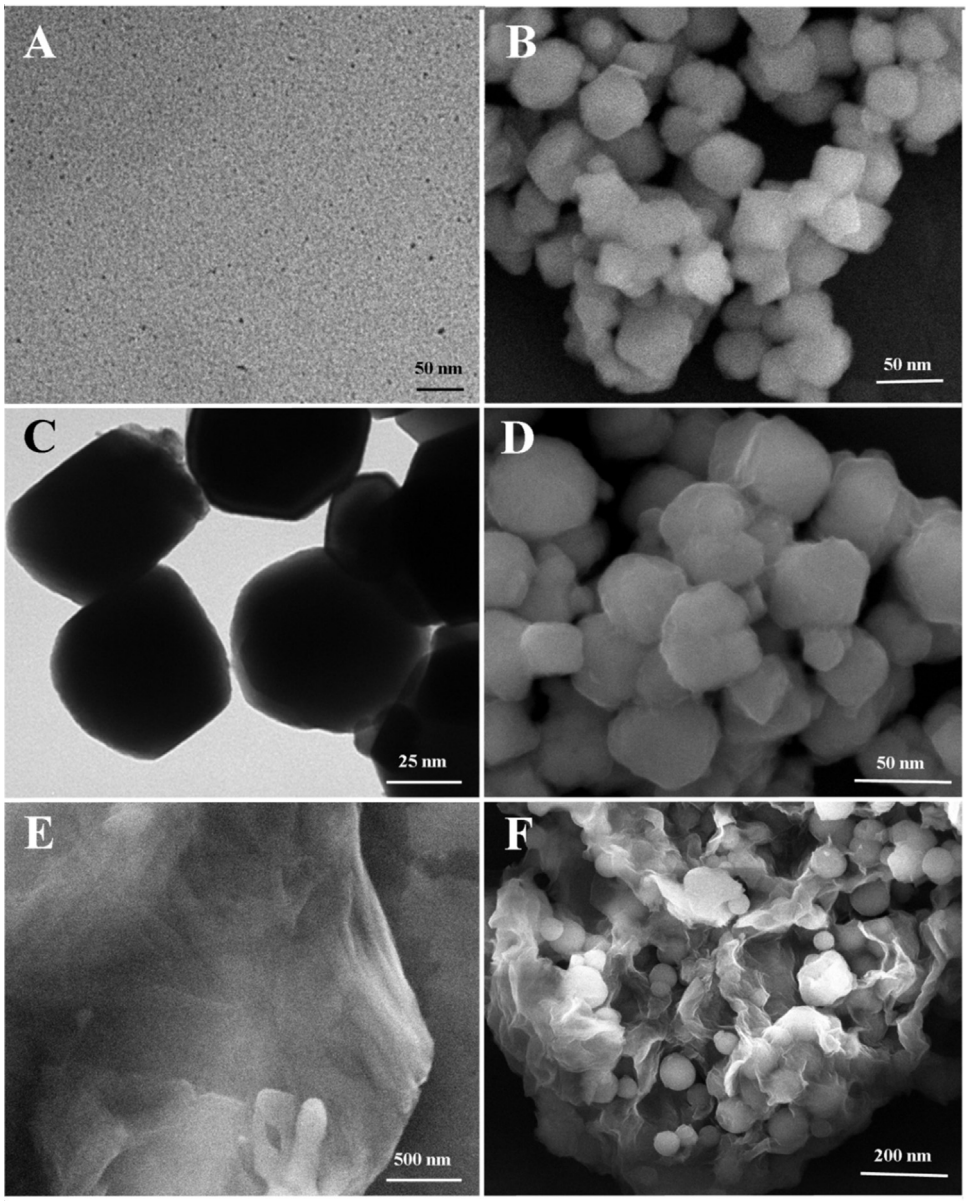

Fig. 3. The TEM images of CQDs (A) and GO@Fe_3O_4 (C); SEM images of Fe_3O_4 (B), GO@Fe_3O_4 (D), GO (E) and GO@Fe_3O_4@β-CD (F).

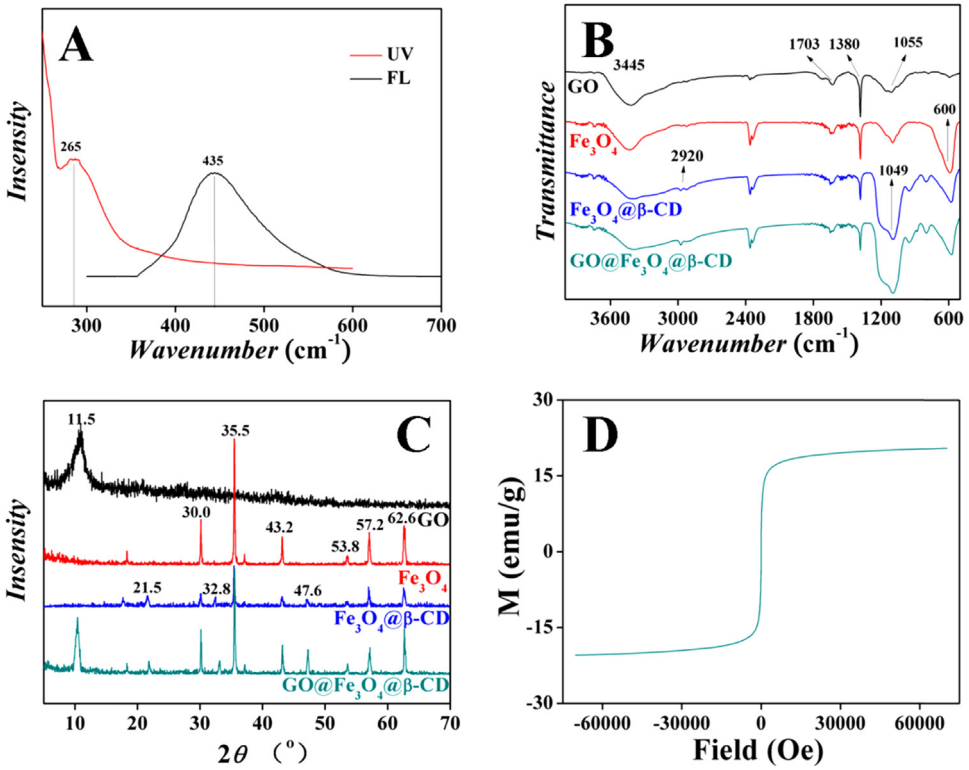

Fig. 4. The UV and FL characterization of CQDs (A); the FTIR (B) and XRD (C) of GO, Fe_3O_4, Fe_3O_4@β-CD and GO@Fe_3O_4@β-CD; the VSM magnetization curves of GO@Fe_3O_4@β-CD (D).

and 2920 cm^{-1} are the stretching vibration absorption peak of C-O and the anti-stretching vibration absorption peak of -CH_2, respectively, which indicated that Fe_3O_4@β-CD was successfully synthesized. In the spectrum of GO@Fe_3O_4@β-CD, it also contained the characteristic absorption peaks of GO and GO@Fe_3O_4@β-CD, which clarified that GO@Fe_3O_4@β-CD was synthesized definitely.

To provide further illustration, the as-prepared GO, Fe_3O_4, Fe_3O_4@β-CD and GO@Fe_3O_4@β-CD were investigated by XRD characterization and they were shown in Fig. 4(C). Obviously, the characteristic peak of GO situated around $2\theta = 11.5^{\circ}$ and the characteristic peak of Fe_3O_4 were at $2\theta = 30.0^{\circ}$, 35.5°, 43.2°, 53.8°, 57.2° and 62.6°, respectively. In the spectrum of Fe_3O_4@β-CD, some new diffraction peaks appear at 21.5°, 32.8° and 47.6°, which are the characteristic peaks of β-CD, indicating that β-CD was successfully coated on the surface of Fe_3O_4. In detail, all of the diffraction peaks could be observed in the pattern of GO@Fe_3O_4@β-CD, and the satisfying results further provided remarkable support that GO@Fe_3O_4@β-CD was successful prepared.

And Fig. 4(D) showed that vibration sample magnetometer (VSM) magnetization curves of GO@Fe_3O_4@β-CD. The saturation magnetization of CS@Fe_3O_4@GO was 18.5 emu/g, which was sufficient to meet the needs of the magnetic separation.

3.2. Immobilization/adsorption properties study

To illustrate the excellent immobilization property of GO@Fe_3O_4@β-CD, the immobilization capacities of GO@Fe_3O_4@β-CD, magnetic graphene oxide (MGO, prepared by our previous work [52]) and Fe_3O_4@β-CD for A-Apt were compared and measured, shown in Fig. 5(A, B). The immobilization capacities for A-Apt at different initial concentrations, i.e. the immobilization isotherms, are shown in Fig. 5(A). The immobilization capacity (Q) of these materials for A-Apt was all increased with the increase of A-Apt concentration (c) before reaching the maximum capacities. The immobilization capacity of GO@Fe_3O_4@β-CD was 1.65×10^{-10} mol/mg while MGO of 1.25×10^{-10} mol/mg and Fe_3O_4@β-CD of 9.50×10^{-11} mol/mg. Fig. 5(B) showed the immobilization kinetics for A-Apt. GO@Fe_3O_4@β-CD could reach maximum immobilization easily within 15 min compared with MGO of 20 min and Fe_3O_4@β-CD of 25 min. These satisfied results of GO@Fe_3O_4@β-CD presented may contribute to the stronger π-π stacking effect between GO@Fe_3O_4@β-CD and A-Apt.

The adsorption performance of GO@Fe_3O_4@β-CD@A-Apt to CQDs-ssDNA was measured and shown in Fig. 5(C, D). The adsorption capacities for CQDs-ssDNA at different initial concentrations, i.e. the adsorption isotherms, are shown in Fig. 5(C). The adsorption capacity (Q') for CQDs-ssDNA increased with the increase of CQDs-ssDNA concentration (c') before reaching a maximum of 1.55×10^{-10} mol/mg. Fig. 5(D) showed the adsorption kinetics of GO@Fe_3O_4@β-CD@A-Apt for CQDs-ssDNA. GO@Fe_3O_4@β-CD@A-Apt could reach maximum adsorption easily within 15 min that can be contributed to the electrostatic interaction and fast mass transfer between GO@Fe_3O_4@β-CD@A-Apt and CQDs-ssDNA.

3.3. Optimization of the CL biosensor

The solution flow rate in peristaltic pumps was an important parameter for the adsorption time and the amount of CQDs-ssDNA in the solution or absorbed on the GO@Fe_3O_4@β-CD@A-Apt. When the solution flow rate was too high, CQDs-ssDNA could not be absorbed by GO@Fe_3O_4@β-CD@A-Apt effectively. But when the solution flow rate was too low, the other substances in the samples solution would be absorbed by GO@Fe_3O_4@β-CD@A-Apt and may interfere with samples' detection. Thus, the solution flow rate in main pump of 1.69 mL/min and the solution flow rate in vice pump of 1.45 mL/min were optimized for further work between 1.00 mL/min and 2.50 mL/min. In addition, the concentrations of luminol, H_2O_2 and NaOH would also affect the CL intensity and these were chosen as showed in Fig. 6(A–C). It could be seen that the maximum CL intensity could be obtained at the concentration of luminol: 5.0×10^{-4} mol/L, H_2O_2: 0.1 mol/L and NaOH:

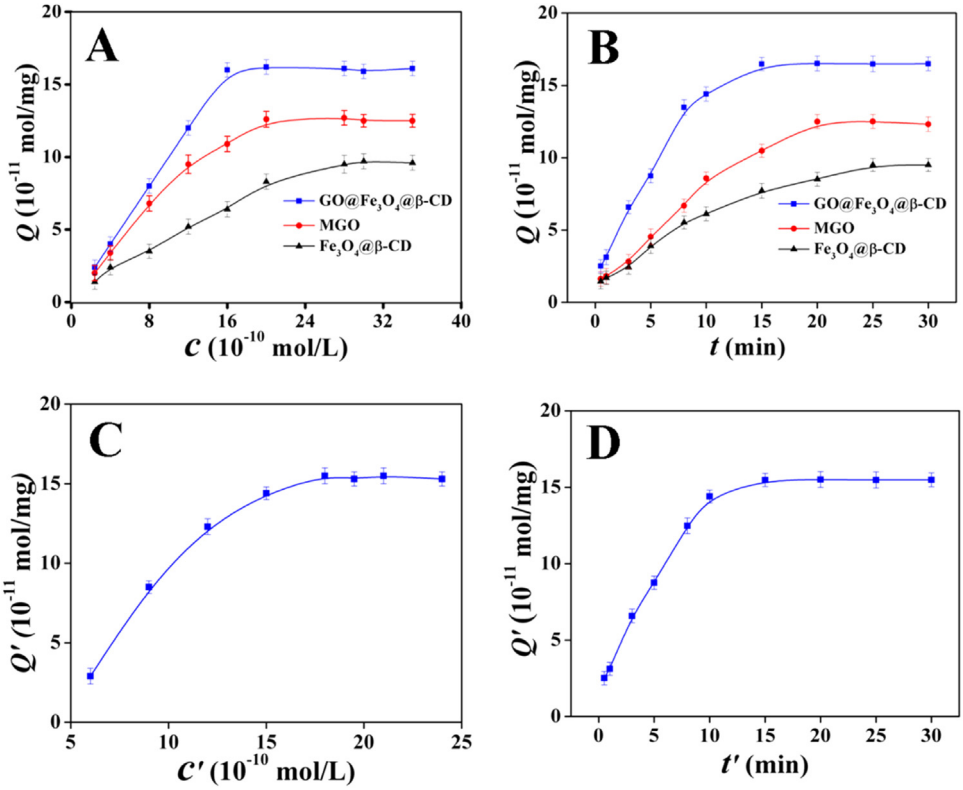

Fig. 5. Immobilization isotherm curves (A), immobilization kinetics curves (B) of GO@Fe_3O_4@β-CD to A-Apt; adsorption isotherm curves (C) and adsorption kinetics curves (D) of GO@Fe_3O_4@β-CD@A-Apt to CQDs-ssDNA.

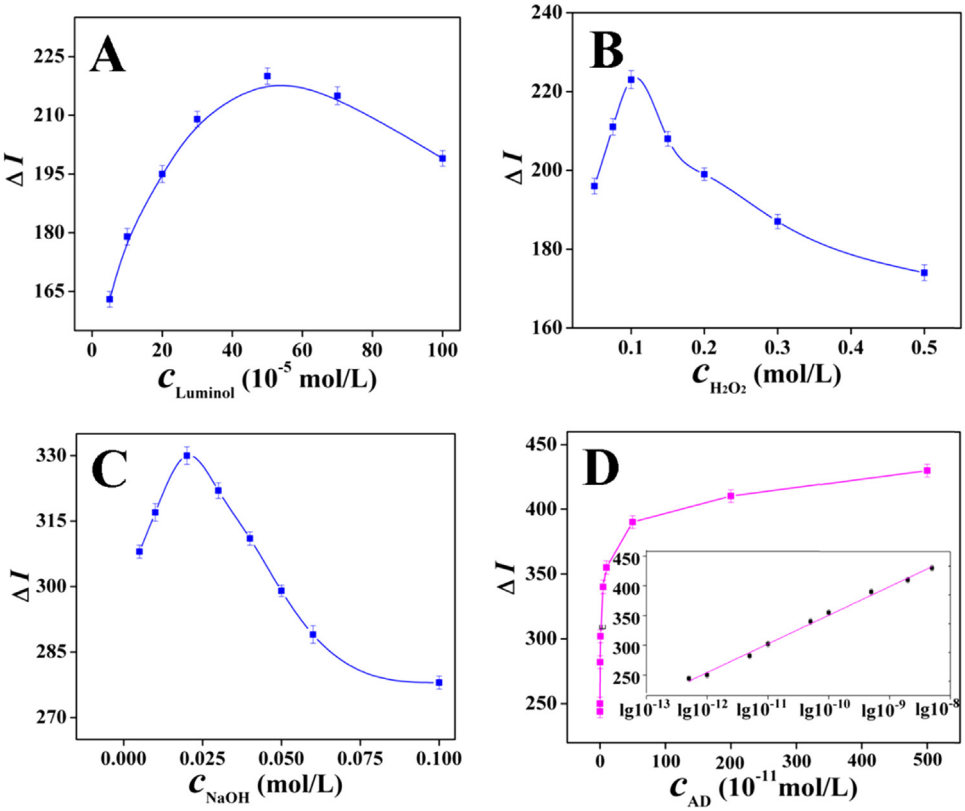

Fig. 6. The CL intensity effects of luminol (A), H_2O_2 (B), NaOH (C) concentrations and the regression equation (D) of the GO@Fe_3O_4β-CD@A-Apt@CQDs-ssDNA - CL biosensor.

Table 1
Comparing results with conventional methods.

Analytical method	Linear range (mol/L)	Detection limit (mol/L)
Proposed	5.0×10^{-13}–5.0×10^{-9}	2.1×10^{-13}
[5]	5.0×10^{-8} –6.0×10^{-6}	1.7×10^{-8}
[6]	10^{-7}–10^{-2}	–
[7]	5.0×10^{-11}–2.0×10^{-8}	3.2×10^{-11}
[8]	3.33×10^{-10}–1.67×10^{-7}	2.17×10^{-10}
[9]	2.30×10^{-8}–1.46×10^{-7}	9.3×10^{-9}
[10]	2.5×10^{-7}–1.0×10^{-4}	2.5×10^{-7}
[11]	6.0×10^{-9}–1.15×10^{-7}	1.8×10^{-9}
[12]	4.0×10^{-7}–1.0×10^{-5}	8.0×10^{-8}

0.02 mol/L, simultaneously.

3.4. Analytical performance of the CL biosensor

Under the optimized conditions, the analytical performance of the proposed GO@Fe_3O_4@β-CD@A-Apt@CQDs-ssDNA-CL biosensor was studied. In Fig. 6(D), it could be seen that the CL intensity (ΔI) and the logarithm of adenosine concentration (lg c_{AD}) showed a good linear correlation. The calibration curve was $\Delta I = 833.86 + 48.30 \lg c_{AD}$ (c_{AD}: mol/L, $R = 0.995$). The detection range of adenosine was 5.0×10^{-13}–5.0×10^{-9} mol/L and the detection limit was 2.1×10^{-13} mol/L (3δ). Simultaneously, the adenosine samples with same concentration were subjected to parallel experiments and the relative standard deviation (RSD) was obtained of 1.4% ($n = 11$). The proposed method was compared with other already existed methods and those results were shown in Table 1. The prepared CL biosensor exhibited a relatively wide linear range and low detection limit to the detection of adenosine.

3.5. Selectivity performance of the CL biosensor

Interference experiments were performed to evaluate the selectivity of the GO@Fe_3O_4@β-CD@A-Apt@CQDs-ssDNA - CL biosensor for AD. In experiments, different analytes were added in standard AD solution. The concentrations of analytes were higher than that in real urine samples and these analytes involved UA, Cr, Gly, L-Cys, AC, LA, K^+ and Cl^-. The anti-interference ability was compared with the conventional CL method, shown in Fig. 7(A). These experimental conditions between the proposed CL biosensor and the conventional CL sensor were the same, except the addition of GO@Fe_3O_4@β-CD@A-Apt. In the proposed CL biosensor, 350 interference multiples of Cr would interfere the determination of AD. Compared to the conventional CL sensor (30 multiples), the anti-interference ability of the proposed CL biosensor had relatively increases. These similar conclusions were applied to Cr, Gly, L-Cys and LA. But comparing with other analytes, the increases of AC was not significant, which may because AC had similar structural units with AD. For other interferences-inorganic ions, the prepared CL biosensor also exhibited obviously anti-jamming capability compared to conventional CL sensor, which may also due to the weak structural similarity. Therefore, the proposed GO@Fe_3O_4@β-CD@A-Apt@CQDs-ssDNA-CL biosensor demonstrated a strong ability to resist interferences and was suitable for the detection of AD.

3.6. Recyclability of the CL biosensor

The repeatability of the synthetic polymers is one of the important parameters to evaluate the performance of a biosensor. In the GO@Fe_3O_4@β-CD@A-Apt@ CQDs-ssDNA-CL biosensor, when a test was completed, GO@Fe_3O_4@β-CD could be recycled for reuse. When AD existed in the sample solutions, GO@Fe_3O_4@β-CD@A-Apt@AD compound was formed. But when the conditions change, such as highly acidic environment, A-Apt would hydrolyze and A-Apt@AD was released from the surface of GO@Fe_3O_4@β-CD. After magnetic separation, GO@Fe_3O_4@β-CD could be reused to fix A-Apt in the construction of the CL biosensor. As shown in Fig. 7(B), the adsorption capacity of GO@Fe_3O_4@β-CD that was used 6 times was 1.52×10^{-10} mol/mg compared with the adsorption capacity (1.65×10^{-10} mol/mg) of GO@Fe_3O_4@β-CD before any use. The result showed that there was 7.9% adsorption capacity loss in 6 times. It manifested that GO@Fe_3O_4@β-CD was suitable to be reused in the CL biosensor.

3.7. Application of the CL biosensor

As is shown in Table 2, under the optimal experimental conditions, the GO@Fe_3O_4@β-CD@A-Apt@CQDs-ssDNA - CL biosensor was applied in practical urine samples. The human urine samples were collected from six healthy individuals (3 male and 3 female) and were diluted 1000-fold with water, respectively, to avoid too high concentration beyond the detection range of AD. The AD concentrations in urine samples were calculated as $(6.5 \pm 0.3) \times 10^{-7}$ mol/L by a standard addition method and there was no significant difference in concentration between male and female urine samples, which were comparable to the literature values for AD in human healthy controls [53]. To calculate the recoveries, urine samples were then spiked with 5.0×10^{-10} mol/L of AD, respectively. As shown in Table 2, the proposed method shows excellent recoveries in the range 98.6–101.0%. These results showed that the CL biosensor had good accuracy in the determination of AD.

To further support the performance of the analytical procedure, some validation experiments were carried out. As was shown in Table 3, under the optimal experimental conditions, the proposed method and drug standard method – HPLC [54] were all applied to determinate AD in the same standard samples, respectively. Obviously, the recoveries of the proposed method varied from 99.8% to 100.6% compared with the recoveries of the drug standard method varied from 99.8% to 100.4%.

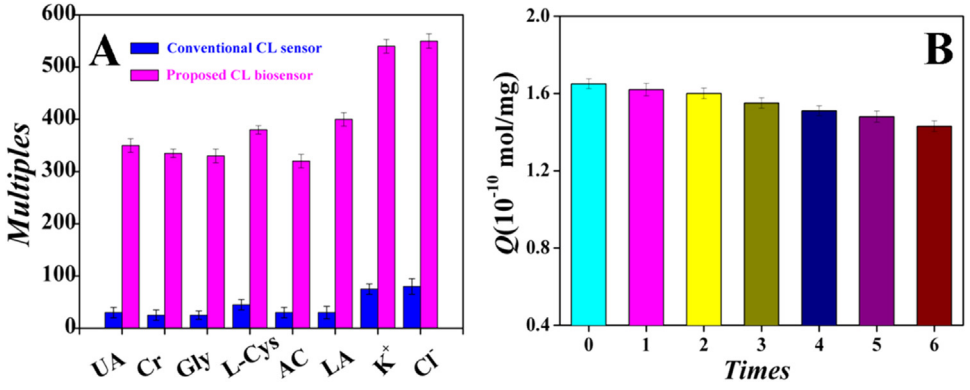

Fig. 7. The interference study (A) and the recyclability times (B) of the GO@Fe_3O_4@β-CD@A-Apt@CQDs-ssDNA-CL biosensor.

Table 2
Application of the proposed CL biosensor. Male urine samples: 1–3; female urine samples: 4–6.

Sample	c (10^{-10} mol/L) (n = 6)	c_{added} (10^{-10} mol/L)	c_{found} (10^{-10} mol/L) (n = 6)	RSD (%)	Recovery (%)
1	6.47	5.00	11.40	2.43	98.6
2	6.50	5.00	11.51	3.42	100.2
3	6.51	5.00	11.47	2.80	99.2
4	6.49	5.00	11.54	2.29	101.0
5	6.50	5.00	11.52	3.26	100.4
6	6.47	5.00	11.46	3.40	99.8

Table 3
Validation experiments of the analytical procedure. the proposed method: samples 1–3; the drug standard method: samples 1′–3′.

Sample	c (10^{-10} mol/L) (n = 6)	c_{added} (10^{-10} mol/L)	c_{found} (10^{-10} mol/L) (n = 6)	RSD (%)	Recovery (%)
1	6.53	5.00	11.52	2.2	99.8
1′	6.50	5.00	11.49	1.6	99.8
2	6.48	5.00	11.50	2.0	100.4
2′	6.51	5.00	11.51	2.8	100.0
3	6.54	5.00	11.57	2.3	100.6
3′	6.48	5.00	11.50	2.6	100.4

These results showed that the proposed method had relatively good accuracy in the determination of AD compared to the national identification of standard method. Therefore, the proposed CL biosensor provides the possibility of measuring AD in practical urine samples and it may be further applied to detect other more complex samples that need to be more studied.

3.8. Construction principle and possible catalytic mechanism of the CL biosensor

During construction of the GO@Fe_3O_4@β-CD@A-Apt@CQDs-ssDNA - CL biosensor, GO@Fe_3O_4@β-CD was regarded as a supporting material and A-Apt as a specific recognition element. As showed in Fig. 2, primitively, A-Apt was immobilized on the surface of GO@Fe_3O_4@β-CD by the π-π stacking effect between GO@Fe_3O_4@β-CD and A-Apt. Then the CQDs-ssDNA could be adsorbed on the surface of the GO@Fe_3O_4@β-CD@A-Apt by base complementary pairing between A-Apt and CQDs-ssDNA to form the base-supported chain-like composites – GO@Fe_3O_4@β-CD@A-Apt@CQDs-ssDNA. When AD presented in the solution, AD and A-Apt were bound together specifically, making the CQDs-ssDNA desorb from the surface of GO@Fe_3O_4@β-CD@A-Apt. Ultimately, GO@Fe_3O_4@β-CD@A-Apt@AD was separated by an external magnetic field and CQDs-ssDNA was desorbed to solution. CQDs-ssDNA in solution would induce the CL signal changes of luminol – H_2O_2 – NaOH system and realized the quantitative detection of AD. So the GO@Fe_3O_4@β-CD@A-Apt/CQDs-ssDNA-CL biosensor was constructed to achieve highly selective and sensitive detection of AD.

In the CL system of luminol – H_2O_2 – NaOH, H_2O_2 can oxidize luminol in alkaline environment and produces luminescence. But the CL intensity of the single reaction is relatively slow. As mentioned in the Introduction, as a catalyst, CQDs can catalyze some CL systems. In the proposed CL biosensor, the possible mechanism of CQDs-ssDNA catalyzing the CL system of luminal – H_2O_2 – NaOH is as follows (Fig. 8): under alkaline conditions, luminol is oxidized by H_2O_2 to produce luminol acid radical ion (A). At the same time, the CQDs-ssDNA gain the energy that is released from the interaction of H_2O_2 and CQDs-ssDNA and turn into CQDs*-ssDNA (B). Under the reaction of A and B, A can be further oxidized by synergy to promote the formation of intermediates and then generate C, which significantly increases the CL intensity. These possible CL mechanisms were consistent with the mechanism of the literatures [25,55].

4. Conclusions

As an important intermediate, a participant in the body's activities and a potential biomarker of cancers or tumors, the accurate, sensitive and selective detection of AD is of great significance. In the GO@Fe_3O_4@β-CD@A-Apt@CQDs-ssDNA-CL biosensor, the base-supported chain-like composites – GO@Fe_3O_4@β-CD@A-Apt@CQDs-ssDNA were successfully prepared and were used to construction of the CL biosensor. GO@Fe_3O_4@β-CD with the good biocompatibility and large specific surface area provided large binding sites to A-Apt. As a specific recognition element, A-Apt significantly improved the selectivity of CL methods owing to the specific recognition ability between aptamers and target molecules. In addition, CQDs-ssDNA effectively catalyzed the CL system of luminal – H_2O_2 – NaOH and further improved the detection sensitivity. The prepared CL biosensor for AD detection showed high sensitivity with detection limit of 2.1×10^{-13} mol/L, wide linear range of 5.0×10^{-13}–5.0×10^{-9} mol/L and recoveries in the range 98.6–101.0%. So the proposed GO@Fe_3O_4@β-CD@A-Apt@CQDs-ssDNA-CL biosensor provided a potential application value for AD detection in simple samples, such as urine and serum, which contain a certain amount of adenosine, have convenient sources, and are generally used as hospital sampling.

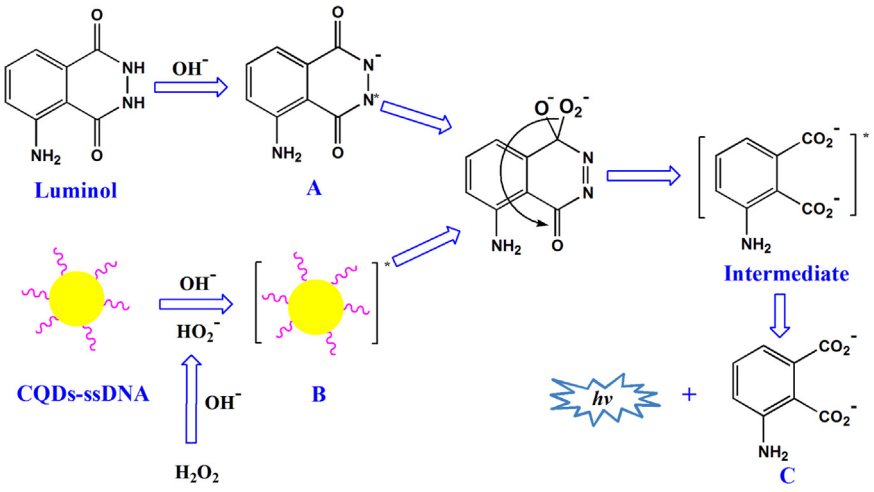

Fig. 8. The possible chemiluminescence mechanism of the CL biosensor.

Acknowledgements

This work was supported by the Shandong Provincial Natural Science Foundation of China (No. ZR2016BM01) and Horizontal Scientific Research Project of China (No. W15077).

References

[1] A.N. Drury, A. Szent-Györgyi, The physiological activity of adenine compounds with especial reference to their action upon the mammalian heart, J. Physiol. 68 (3) (1929) 213–237.
[2] O. Andersson, Role of adenosine signalling and metabolism in beta-cell regeneration, Exp. Cell Res. 321 (1) (2014) 3–10.
[3] L. Antonioli, C. Blandizzi, P. Pacher, G. Haskó, Immunity, inflammation and cancer: a leading role for adenosine, Nat. Rev. Cancer 13 (2013) 842–857.
[4] A. Bahreyni, S.S. Samani, E. Ghorbani, F. Rahmani, R. khayami, et al., Adenosine: an endogenous mediator in the pathogenesis of gynecological cancer, J. Cell. Physiol. (2017), http://dx.doi.org/10.1002/jcp.26056.
[5] L. Xu, X. Shen, B. Li, C. Zhu, X. Zhou, G-quadruplex based Exo III-assisted signal amplification aptasensor for the colorimetric detection of adenosine, Anal. Chim. Acta 980 (2017) 58–64.
[6] C. Zhang, B. Man, S. Jiang, C. Yang, M. Liu, et al., SERS detection of low-concentration adenosine by silver nanoparticles on silicon nanoporous pyramid arrays structure, Appl. Surf. Sci. 347 (2015) 668–672.
[7] J. Shen, H. Wang, C. Li, Y. Zhao, X. Yu, et al., Label-free electrochemical aptasensor for adenosine detection based on cascade signal amplification strategy, Biosens. Bioelectron. 90 (2017) 356–362.
[8] Y. Song, T. Tang, X. Wang, G. Xu, F. Wei, et al., Highly selective and sensitive detection of adenosine utilizing signal amplification based on silver ions-assisted cation exchange reaction with CdTe quantum dots, Sens. Actuators B: Chem. 247 (2017) 305–311.
[9] Z. Hashemian, T. Khayamian, M. Saraji, M.P. Shirani, Aptasensor based on fluorescence resonance energy transfer for the analysis of adenosine in urine samples of lung cancer patients, Biosens. Bioelectron. 79 (2016) 334–340.
[10] R.M. Marin, K.G. Franchini, S.A. Rocco, Analysis of adenosine by RP-HPLC method and its application to the study of adenosine kinase kinetics, J. Sep. Sci. 30 (15) (2007) 2473–2479.
[11] J. Zhang, Y. Wang, Y. He, T. Jiang, H. Yang, et al., Determination of urinary adenosine using resonance light scattering of gold nanoparticles modified structure-switching aptamer, Anal. Biochem. 397 (2010) 212–217.
[12] X. Yan, Z. Cao, M. Kai, J. Lu, Label-free aptamer-based chemiluminescence detection of adenosine, Talanta 79 (2) (2009) 383–387.
[13] Z. Chu, L. Zhang, Y. Huang, S. Zhao, G-quadruplex DNAzyme chemiluminescence aptasensor based on the target triggered DNA recycling for sensitive detection of adenosine, Anal. Methods 6 (11) (2014) 3700–3705.
[14] N. Siraj, B. El-Zahab, S. Hamdan, T.E. Karam, L.H. Haber, et al., Fluorescence, phosphorescence, and chemiluminescence, Anal. Chem. 88 (2016) 170–202.
[15] X. Ji, W. Wang, X. Li, Y. Chen, C. Ding, Enhanced chemiluminescence detection of glutathione based on isoluminol-PSM nanoparticles probe, Talanta 150 (2016) 666–670.
[16] I. Mortaza, Revisiting flow-chemiluminescence techniques: pharmaceutical analysis, Luminescence 28 (6) (2013) 798–820.
[17] J.A. Ocana-Gonzalez, M. Ramos-Payan, R. Fernandez-Torres, M.V. Navarro, M.A. Bello-López, Application of chemiluminescence in the analysis of wastewaters – a review, Talanta 122 (2014) 214–222.
[18] J.L. Adcock, C.J. Barrow, N.W. Barnett, X.A. Conlan, C.F. Hogan, et al., Chemiluminescence and electrochemiluminescence detection of controlled drugs.
[19] H. Chen, Q. Gao, J. Li, J. Lin, Graphene materials-based chemiluminescence for sensing, J. Photochem. Photobiol. C: Photochem. Rev. 27 (2016) 54–71.
[20] H. Yang, L. Li, Y. Ding, D. Ye, Y. Wang, et al., Molecularly imprinted electrochemical sensor based on bioinspired Au microflowers for ultra-trace cholesterol assay, Biosens. Bioelectron. 92 (2017) 748–754.
[21] X. Yi, W. Dong, X. Zhang, J. Xie, Yuming Huang, MIL-53(Fe) MOF-mediated catalytic chemiluminescence for sensitive detection of glucose, Anal. Bioanal. Chem. 408 (30) (2016) 8805–8812 (Email author).
[22] Y. Qi, F. Xiu, M. Zheng, B. Li, A simple and rapid chemiluminescence aptasensor for acetamiprid in contaminated samples: sensitivity, selectivity and mechanism, Biosens. Bioelectron. 83 (2016) 243–249.
[23] M. Liu, H. Zhang, J. Shu, X. Liu, F. Li, et al., Gold nanoparticles bifunctionalized by chemiluminescence reagent and catalyst metal complexes: synthesis and unique chemiluminescence property, Anal. Chem. 86 (6) (2014) 2857–2861.
[24] H. Chen, L. Lin1, H. Li, J. Lin, Quantum dots-enhanced chemiluminescence: mechanism and application, Coord. Chem. Rev. 263–264 (2014) 86–100.
[25] R. Wang, K. Lu, Z. Tang, Y. Xu, Recent progress in carbon quantum dots: synthesis, properties and applications in photocatalysis, J. Mater. Chem. A 5 (2017) 3717–3734.
[26] H. Fu, Z. Ji, X. Chen, A. Cheng, S. Liu, J. You, et al., A versatile ratiometric nanosensing approach for sensitive and accurate detection of Hg^{2+} and biological thiols based on new fluorescent carbon quantum dots, Anal. Bioanal. Chem. 409 (9) (2017) 2373–2382.
[27] Y. Dong, Y. Peng, J. Wang, C. Wang, Determination of cytochrome C based on its enhancing effect on the electrogenerated chemiluminescence of carbon quantum dots, Microchim. Acta 184 (2017) 2089–2095.
[28] Y. Wu, Y.J. Kwon, Aptamers: the "evolution" of SELEX, Methods 106 (2016) 21–28.
[29] R. Huang, Z. Xi, N. He, Applications of aptamers for chemistry analysis, medicine and food security, Sci. China Chem. 58 (7) (2015) 1122–1130.
[30] C. Chandola, S. Kalme, M.G. Casteleijn, A. Urtti, M. Neerathilingam, Application of aptamers in diagnostics, drug-delivery and imaging, J. Biosci. 41 (2016) 535–561.
[31] P. Gai, C. Gu, T. Hong, F. Li, Ultrasensitive self-powered aptasensor based on enzyme biofuel cell and DNA bioconjugate: a facile and powerful tool for antibiotic residue detection, Anal. Chem. 89 (3) (2017) 2163–2169.
[32] Y. Hou, J. Liu, M. Hong, X. Li, Q. Yue, et al., A reusable aptasensor of thrombin based on DNA machine employing resonance light scattering technique, Biosens. Bioelectron. 92 (2017) 259–265.
[33] B. Liu, J. Xie, H. Ma, X. Zhang, Y. Pan, et al., From graphite to graphene oxide and graphene oxide quantum dots, Small 13 (18) (2017) 16–22.
[34] B.C. Thompson, E. Murray, G.G. Wallace, Graphite oxide to graphene. biomaterials to bionics, Adv. Mater. 27 (46) (2015) 7563–7582.
[35] Y. Zhu, S. Murali, W. Cai, X. Li, J.W. Suk, et al., Graphene and graphene oxide: synthesis, properties, and applications, Adv. Mater. 32 (2010) 3906–3924.
[36] V. Chabot, D. Higgins, A. Yu, X. Xiao, Z. Chen, et al., A review of graphene and graphene oxide sponge: material synthesis and applications to energy and the environment, Energy Environ. Sci. 7 (2014) 1564–1596.
[37] S.S. Nanda, G.C. Papaefthymiou, D.K. Yi, Functionalization of graphene oxide and its biomedical applications, Crit. Rev. Solid State Mater. Sci. 40 (2015) 291–315.
[38] G. Eda, M. Chhowalla, Chemically derived graphene oxide: towards large-area thin-film electronics and optoelectronics, Adv. Mater. 22 (22) (2010) 2392–2415.
[39] J. Lee, J. Kima, S. Kima, D.H. Min, Biosensors based on graphene oxide and its biomedical application, Adv. Drug Deliv. Rev. 105 (2016) 275–287.
[40] K. Ling, H. Jiang, Y. Li, X. Tao, C. Qiu, et al., A self-assembling RNA aptamer-based graphene oxide sensor for the turn-on detection of theophylline in serum, Biosens. Bioelectron. 86 (2016) 8–13.
[41] J. Song, J. Yang, J. Zeng, J. Tan, L. Zhang, Graphite oxide film-modified electrode as an electrochemical sensor for acetaminophen, Sens. Actuators B: Chem. 155 (1) (2011) 220–225.
[42] T. Endo, Large-ring cyclodextrins, Trends Glycosci. Glycotechnol. 23 (2011) 79–92.
[43] P. Ivano, Further studies on the conformations of large-ring cyclodextrins, Bulg. Chem. Commun. 46 (2014) 238–245.
[44] Y. Bai, X. Fan, C. Mu, Z. Yang, D. Wang, et al., Cyclodextrin-based topological macromolecules, Prog. Chem. 25 (2–3) (2013) 363–369.
[45] B. Gidwani, A. Vyas, Synthesis, characterization and application of epichlorohydrin-beta-cyclodextrin polymer, Colloids Surf. B: Biointerfaces 114 (2014) 130–137.
[46] N. Morin-Crini, G. Crini, Environmental applications of water-insoluble beta-cyclodextrin-epichlorohydrin polymers, Prog. Polym. Sci. 38 (2) (2013) 344–368.
[47] N. Erdogar, G. Varan, E. Bilensoy, Amphiphilic cyclodextrin derivatives for targeted drug delivery to tumors, Curr. Top. Med. Chem. 17 (13) (2017) 1521–1528.
[48] J.M. Casas-Solvas, E. Ortiz-Salmerón, I. Fernández, L. García-Fuentes, F. Santoyo-González, et al., Ferrocene-beta-cyclodextrin conjugates: synthesis, supramolecular behavior, and use as electrochemical sensors, Chem. – Eur. J. 15 (33) (2009) 8146–8162.
[49] W.S. Hummers, R.E. Offeman, Preparation of graphitic oxide, J. Am. Chem. Soc. 80 (1958) 1339.
[50] H. Duan, X. Wang, Y. Wang, Y. Sun, C. Luo, et al., An ultrasensitive lysozyme chemiluminescence biosensor based on surface molecular imprinting using ionic liquid modified magnetic graphene oxide/beta-cyclodextrin as supporting material, Anal. Chim. Acta 918 (2016) 89–96.
[51] Li Guo, Y. Zhang, W. Li, Sustainable microalgae for the simultaneous synthesis of carbon quantum dots for cellular imaging and porous carbon for CO_2 capture, J. Colloid Interface Sci. 493 (2017) 257–264.
[52] Y. Sun, Y. Wang, J. Li, C. Ding, C. Luo, et al., An ultrasensitive chemiluminescence aptasensor for indirect hemin detection based on aptamer recognition materials, New J. Chem. 41 (2017) 6098–6104.
[53] Y. Zheng, G. Xu, D. Liu, J. Xiong, P. Zhang, et al., Study of urinary nucleosides as biological marker in cancer patients analyzed by micellar electrokinetic capillary chromatography, Electrophoresis 23 (2002) 4104–4109.
[54] National Pharmacopoeia Committee, Pharmacopoeia of People's Republic of China [M]. Part2: Appendix 591, 2000.
[55] Z. Yan, Y. Yu, J. Chen, Glycine-functionalized carbon quantum dots as chemiluminescence sensitization for detection of m-phenylenediamine, Anal. Methods 7 (2015) 1133–1139.